

1 **A 60-year record of atmospheric carbon monoxide reconstructed from Greenland**  
2 **firn air: SUPPLEMENTARY MATERIAL**

3  
4 **2. Sampling and Analytical Methods**

5  
6 We provide some further detail here on NOAA [CO] and [H<sub>2</sub>] analyses, since up-to-date  
7 descriptions are not available elsewhere. [CO] was measured on a system designed to  
8 analyze a suite of trace gases in the same air sample. Sample flasks were first attached to  
9 an eight port sampling manifold fitted with all stainless steel components. The dead  
10 volume between flasks and a down-line transfer pump was then evacuated to < 0.13  
11 mbar. A stream selection valve determines which flask is opened to the system and a  
12 transfer pump with a MFC regulates flow rates. Samples are cryogenically dried to -80 C  
13 before a second stream selection valve partitions air flow to the CO analyzer and three  
14 other instruments. Sample flow rates, stream selection valves and instrument functions  
15 are controlled by HP computer and custom software  
16 ([http://www.esrl.noaa.gov/gmd/outreach/behind\\_the\\_scenes/measurementlab.html](http://www.esrl.noaa.gov/gmd/outreach/behind_the_scenes/measurementlab.html)).

17 Sample metadata and digitalized instrument response are archived. [CO] is calculated in  
18 units of nmol mol<sup>-1</sup>.

19  
20 Instruments (Reducing Gas Analyzer) from Trace Analytical Inc. were calibrated using  
21 six reference gases evenly spaced between 50 to 200 nmol mol<sup>-1</sup> [CO]. Instrument  
22 response over this range was defined by a quadratic function. The VURF instruments  
23 were linear over the atmospheric range and therefore the calibration consisted of a single  
24 reference gas (~300 nmol mol<sup>-1</sup>) and a blank (UHP zero air run through a trap containing  
25 Schutze reagent). Reference gases are tied to the WMO-2004 [CO] scale. The scale is  
26 based upon six sets of primary CO-in-air mixtures prepared using gravimetric techniques  
27 (Novelli et al., 1991) and has undergone revision to address drift with time (Novelli et al.,  
28 2003).

29  
30 An informal comparison of [H<sub>2</sub>] measurements in 2008 between the Max-Planck Institute  
31 for Biogeochemistry (MPI-BGC) and NOAA showed a difference of 9 nmol mol<sup>-1</sup> over  
32 the range 470 to 560, with NOAA low. The MPI-BGC acts as the World Calibration  
33 Center for WMO/GAW H<sub>2</sub> reference gases.

34  
35 Table S2 shows the data from the field procedural blank tests for the US and EU firn air  
36 systems (analyzed at NOAA). Pairs of flasks were filled using each system to test the  
37 system blanks. The average US system [CO] blank is -0.4 ppb, and the average EU  
38 system blank is + 0.5 ppb which are both smaller than the estimated NOAA measurement  
39 uncertainty (1.2 ppb). The US system [H<sub>2</sub>] blank is 4.8 ppb (compared to measurement  
40 1σ uncertainty of 4.0 ppb), and the EU system [H<sub>2</sub>] blank is 6.1 ppb.

41  
42 Figure S1 shows the [CO] and [H<sub>2</sub>] comparisons of surface flasks filled through the firn  
43 air systems with NOAA flask measurements from the two closest monitoring stations  
44 during the same time period. All air samples shown (firn surface and NOAA) were taken  
45 using identical 2.5L glass flasks and were measured at NOAA. As can be seen, [CO] and  
46 [H<sub>2</sub>] in surface air sampled with firn air systems at all sites are within the range expected

1 from the nearest NOAA flask collection sites, Summit (72.58°N, 38.46°W) and Alert  
2 (82.45°N, 62.51°W).

### 3.1 NEEM 2008 Firn Air Data

7 The UEA [CO] and [H<sub>2</sub>] data from the S4 borehole were excluded from the final  
8 combined data sets primarily because we have determined that it is best to treat each  
9 borehole separately for the reconstructions (see main text), and the S4 borehole did not  
10 sample the oldest air and did not have enough supporting trace gas measurements to  
11 constrain the depth-diffusivity profiles (see Section 4.1) as well as in the EU and US  
12 boreholes. In the top  $\approx 30$  m, this borehole also appears to be affected by unusually fast  
13 gas exchange with surface air, probably due to the adjacent ( $\approx 15$ m) open US borehole.  
14 Finally, the UEA [CO] data are nominally on the WMO 2004 [CO] scale, same as the  
15 NOAA data, yet we observe an unexplained offset (UEA  $\approx 9$  ppb lower) from the NOAA  
16 data even for depths below 30 m. A single sample from the S3 borehole was also  
17 collected with the UEA high-volume system at 75.1 m depth. This sample was not  
18 included in the final combined data set because of the same unexplained apparent [CO]  
19 scale offset as for the borehole S4 samples.

21 Stony Brook [CO] data were excluded because of relatively large analytical uncertainties.  
22 Heidelberg [H<sub>2</sub>] data were excluded because the data set was clearly more noisy than the  
23 NOAA or CSIRO data, suggesting issues during flask storage or analysis.

25 In order to combine the different sets of firn measurements, they must first be placed on  
26 the same calibration scale. Calibration offsets for both [CO] and [H<sub>2</sub>] between different  
27 laboratories are imperfectly characterized, however. For this reason we chose to use the  
28 NEEM data themselves to calculate the calibration offsets. Individual offsets were  
29 determined for each available depth level in each borehole as NOAA - Heidelberg and  
30 NOAA - CSIRO differences. The average of the NOAA - Heidelberg and NOAA -  
31 CSIRO offsets was then used to adjust the Heidelberg and CSIRO measurements to the  
32 WMO 2004 scale. All the sets of measurements from each borehole were then averaged  
33 (by depth level) to produce the finalized data sets shown in Figure 4. As discussed in the  
34 main text, we are not attempting to reconstruct a true atmospheric history of [H<sub>2</sub>], but  
35 rather using [H<sub>2</sub>] as a source of qualitative information about changes in the CO budget.  
36 For this reason, the inverse modeling for [H<sub>2</sub>] was only done using the EU borehole data;  
37 these are the only finalized [H<sub>2</sub>] data shown in Figure 4.

39 The error bars on the finalized NEEM data sets represent the overall data uncertainties  
40 and were determined as follows. For each depth level in each borehole, all the available  
41 flasks (corrected to the WMO 2004 scale for CO and NOAA scale for H<sub>2</sub>) were  
42 considered. Errors were first calculated for all depth levels with more than one flask  
43 sample as either standard deviation (3 or more flasks) or difference between the flask  
44 values (2 flasks). The average of these errors was then calculated for each species and  
45 each borehole. The final uncertainty for all depth levels with only a single flask is taken

1 as this average. For depth levels with multiple flasks, the final uncertainty was taken as  
2 the larger of this average or the error calculated for that particular depth level.

### 3.3 Is CO well preserved in Greenland firn air?

7 As mentioned in the Introduction, the only firn air record of Northern Hemisphere [CO]  
8 published to-date indicated in-situ CO production in the Devon Ice Cap firn (Clark et al.,  
9 2007). The only reasonable substrate for such CO production, regardless of the exact  
10 mechanism, is trace organic material in the firn (e.g., Colussi and Hoffmann, 2003; Haan  
11 and Raynaud, 1998). Due to the small size of the Devon Ice Cap, the Devon firn air site is  
12 much closer to terrigenous sources of organic material than inland Greenland sites. The  
13 Devon site is also warmer (mean annual temperature -23 °C,) than any of our Greenland  
14 sites (-28.9°C for NEEM (Buizert et al., 2012), -31.5°C for NGRIP (Andersen et al.,  
15 2004) and -31°C for Summit (Grootes et al., 1993)) and contains numerous melt layers  
16 (Clark et al., 2007), both of which may result in higher CO production rates in the ice  
17 depending on the mechanism.

19 Although inland Greenland sites are colder and cleaner with respect to trace organics,  
20 Haan and Raynaud (1998) still found evidence for in-situ CO production in ice below 155  
21 m depth from the Summit region. Ice from shallower depths, however, yielded very  
22 stable [CO] values around 90 nmol mol<sup>-1</sup> prior to 1862 AD and a gradual increase (as  
23 expected from the ramping up of anthropogenic emissions) to 100 nmol mol<sup>-1</sup> by 1905  
24 AD (Haan et al., 1996). Thus, published prior work allows both for the possibility that  
25 Greenland firn air [CO] is well preserved, as well as for the possibility that there is some  
26 alteration of the record.

28 To examine this issue, we first considered the possibility that the [CO] peaks observed in  
29 the lock-in zone at each site are artifacts of in-situ production from an ice layer (or layers)  
30 that is enriched in trace organics. Under this hypothesis, this organic – rich ice layer  
31 would have been deposited at all 3 sites. This hypothesis can be ruled out by comparing  
32 NEEM and NGRIP. At NEEM, the [CO] peak occurs at 70 m, which corresponds to an  
33 ice layer age of 225 years (GICC05modelext-NEEM-1 time scale, unpublished). At  
34 NGRIP, the [CO] peak occurs at 71.75 m, corresponding to an ice layer age of 270 years  
35 (GICC05 age scale, (Vinther et al., 2006)).

37 As discussed in the Introduction, [CO] data for about the last two decades are available  
38 for several Arctic sites from the NOAA global flask network (Novelli et al., 1998). This  
39 presents another opportunity for examining the in-situ production question. We can run  
40 the firn gas transport models (see Section 4 in main text) using the recent NOAA-based  
41 histories and compare the model output with observed values for all boreholes. Such a  
42 comparison is only valid for a limited depth range in the firn, however. Our forward gas  
43 transport models do not do a perfect job with reproducing seasonal signals. For example,  
44 we observed some small mis-matches between data and models for the upper firn even  
45 for a gas with a modest seasonal cycle like CO<sub>2</sub> (Buizert et al., 2012). We estimate that  
46 for [CO], which has a very large seasonal cycle, seasonal effects are significant to a depth

1 of ~40 m. Further, gas ages increase very rapidly in the lock-in zone. This means that in  
2 the lock-in zone, model output is significantly affected by [CO] values in the years prior  
3 to the start of the NOAA measurements. We thus limit our model-data comparison to the  
4 depth range between 40m and the start of the lock-in zone in each borehole.

5  
6 The comparison is presented in Figure S2. We plot model-produced curves from NOAA  
7 Alert, Barrow and Ny Alesund station histories. The NOAA Summit station record is not  
8 used because it is shorter and contains large gaps. As can be seen, model curves match  
9 NGRIP and Summit firn air data well within uncertainties, but there are offsets of up to 5  
10  $\text{nmol mol}^{-1}$  for NEEM, with firn data higher than the model curves.

11  
12 One possible explanation for the 0 - 5  $\text{nmol mol}^{-1}$  elevation of data over the model runs is  
13 that the firn values are weighted toward the winter surface mixing ratios. [CO] has a very  
14 large seasonal cycle over Greenland, with peak values in the winter. Figure S3 shows a  
15 comparison of the [CO] seasonal cycle to the seasonal variability in surface pressure and  
16 wind from the Summit and Humboldt automated weather stations (AWS; Fig. 2). These  
17 two AWSs cover the full geographic range of our firn air sites. The Humboldt AWS was  
18 chosen instead of NEEM because of its longer and more continuous record (NEEM  
19 record only starts in 2007 and does not include most of the winters). As can be seen from  
20 Figure S3, both surface pressure variability and wind speed correlate with [CO]. Both  
21 would be expected to enhance gas exchange between the surface and the upper firn (e.g.,  
22 Colbeck, 1989; Schwander, 1989; Sowers et al., 1992), resulting in an effectively higher  
23 gas diffusivity in the winter.

24  
25 It is also possible that this winter weighting effect is slightly different between our sites  
26 and explains some of the small differences between sites evident in Figures 6 and S2. For  
27 example, NEEM is closer to the Humboldt weather station and therefore likely  
28 experiences higher winds than Summit in the winter. Also, as discussed in the main text,  
29 Summit appears to have a reduced seasonal cycle for [CO] as compared to other sites,  
30 with lower [CO] in the winter. NEEM is approximately mid-way between Summit and  
31 Alert and would likely see higher winter [CO] than Summit. Thus, the winter weighting  
32 effect may result in a slightly higher [CO] recorded in the firn at NEEM than at Summit  
33 and NGRIP, consistent with what Figure 6 shows.

34  
35 One further effect that can influence the data – model comparisons is a likely small drift  
36 in the NOAA [CO] calibration scale over time. This drift is currently being investigated  
37 at NOAA ESRL with the ultimate objective of correcting all the affected data. For  
38 atmospheric data used in this study, values from NOAA measurements prior to 2000 are  
39 likely too low by 2 – 4 ppb. This would affect the data-model comparisons in Figure S2,  
40 making the model curves appear too low for the deepest compared data points. The  
41 calibration scale shift is estimated to have happened gradually between 2000 and 2004,  
42 thus the NGRIP firn data may also be biased low by 2 - 4 ppb. Summit firn data and  
43 NEEM firn data are unaffected by this.

#### 44 45 46 **4.1 Forward modeling**

1  
2 There are some important differences in the ways the LGGE-GIPSA (Witrant et al.,  
3 2011) and the INSTAAR (Buizert et al., 2012) forward models handle gas transport in the  
4 firn. The INSTAAR model includes molecular diffusion (Fick's Law; different for  
5 different gases), eddy diffusion (also parameterized as Fick's law, but same for all gases),  
6 and a downward advection term calculated based on mass conservation. Gravitational  
7 settling is explicitly parameterized in the INSTAAR model by including a  $\Delta Mg/RT$  term  
8 in the gas transport equations (see Buizert et al. (2012) for full gas transport equations).  
9 The model physics are uniform throughout the firn column, and both molecular and eddy  
10 diffusivities are manually tuned at each depth level to give the optimal overall fit for a  
11 suite of reference gas species (Buizert et al., 2012). The INSTAAR model has explicit  
12 time stepping and a depth resolution of 1 m down to 59.5 m, and 0.25m below that level.

13  
14 The LGGE-GIPSA model (Witrant et al., 2011) treats molecular diffusion in a similar  
15 way as the INSTAAR model. It also takes into account an eddy diffusion term in the  
16 upper firn which represents fast ("convective") exchanges with the atmosphere but its  
17 magnitude and vertical structure are different in the two models (Buizert et al., 2012).  
18 The LGGE-GIPSA model does not take into account a similar eddy diffusion term  
19 aiming at representing dispersive transport in the lock-in zone. Because the CO diffusion  
20 coefficient in free air is significantly higher than the one of CO<sub>2</sub>, the relative weights of  
21 molecular and eddy diffusion coefficients in the two models can potentially affect the  
22 consistency of their results. The LGGE-GIPSA model representation of gravitational  
23 settling is based on a quasi-steady-state approximation of Darcy's law, which allows to  
24 predict the location of the lock-in depth. As the LGGE-GIPSA and INSTAAR models  
25 lead to very similar results for  $\delta^{15}\text{N}$  of N<sub>2</sub>, the different formulation of gravitational  
26 setting in the two models does not have a significant impact on the results for CO. The  
27 LGGE-GIPSA model representation of advective transport and bubble closure in the  
28 lock-in zone follows the approach of Rommelaere et al. (1997). Although these processes  
29 are formulated differently in the INSTAAR model, a specific test of these processes in  
30 Buizert et al. (2012) (synthetic scenario IV) showed that the two models produce nearly  
31 equivalent results. The LGGE-GIPSA model uses implicit time stepping and a depth  
32 resolution of 0.2 m throughout the firn.

33  
34 The tuning of diffusivities in each model largely compensates for the differences in  
35 model physics, as demonstrated by the overall similar performance of the models in a  
36 recent intercomparison (Buizert et al., 2012). Further, the fact that our reconstructed [CO]  
37 time trend scenarios can be successfully used in both models to reproduce the firn [CO]  
38 data (see Section 4.2 and Figure S5) shows that the two models perform similarly for CO.

39  
40 Neither model includes thermal fractionation (e.g., Severinghaus et al., 2001) as this  
41 process is not expected to significantly affect CO. Both models use monthly-averaged  
42 atmospheric histories for model – data comparisons such as those shown in Figure S2.  
43 This low temporal resolution of the input histories could affect the model-data fit in the  
44 upper firn to a depth of at least 40 m. Further, neither model explicitly takes into account  
45 synoptic surface pressure variations. The average effective increase in diffusivity due to

1 this process is accounted for by diffusivity tuning, however this could still affect gases  
2 with large seasonal cycles (such as CO), as discussed in Section 3.3 above.

### 4 **5.5 Comparison with H<sub>2</sub> in NEEM firn air**

6 The exact rates of H<sub>2</sub> diffusion in ice are unknown and effects on firn air concentrations  
7 have not been quantified. One expected effect is a slight increase in the effective firn  
8 diffusivities of H<sub>2</sub>, resulting in actual age distributions being younger than those  
9 predicted by our models, particularly in the lock-in zone. An alternative way to  
10 conceptualize this is that the increased effective diffusivity of H<sub>2</sub> would result in a  
11 transient atmospheric [H<sub>2</sub>] peak being recorded (as a peak) deeper in the lock-in zone.

13 Another important effect is an expected progressive enrichment of [H<sub>2</sub>] with depth in the  
14 lock-in zone due to bubble close-off fractionation (Severinghaus and Battle, 2006). For  
15 example, a > 90 ‰ (≈ 9 %) enrichment in the Ne/N<sub>2</sub> ratio was observed at the bottom of  
16 the lock-in zone at South Pole, and Ne and H<sub>2</sub> have a very similar molecular diameter  
17 (Severinghaus and Battle, 2006). Because of the expected enrichment with depth, bubble  
18 close-off fractionation would have the effect of raising [H<sub>2</sub>] and shifting the observed  
19 [H<sub>2</sub>] peak deeper in the lock-in zone.

21 These expected but unquantified H<sub>2</sub> effects in the firn preclude a reliable history  
22 reconstruction at this time. However, both of the described effects are expected to shift  
23 the observed [H<sub>2</sub>] peak deeper in the lock-in zone. In our model history reconstruction,  
24 the atmospheric [H<sub>2</sub>] peak would thus appear older than in reality. So while we cannot  
25 reconstruct a reliable history, we may be able to constrain the oldest possible date of the  
26 atmospheric [H<sub>2</sub>] peak. Figure S6 shows a comparison of [H<sub>2</sub>] and [CO] reconstructions  
27 from the NEEM EU borehole. As can be seen, [H<sub>2</sub>] peaks significantly after [CO], even  
28 though we expect the [H<sub>2</sub>] peak to be old-shifted. This suggests that [CO] and [H<sub>2</sub>]  
29 histories de-couple in the 1970s, which is consistent with the hypothesis of increasing  
30 [OH]. Such a de-coupling is unlikely to be driven by the introduction of catalytic  
31 converters because catalytic converters reduce both CO and H<sub>2</sub> emissions, although they  
32 likely increase the overall H<sub>2</sub>/CO emission ratios from vehicles (Vollmer et al., 2010).

1 **References**

- 2  
3 Andersen, K. K., Azuma, N., Barnola, J. M., Bigler, M., Biscaye, P., Caillon, N.,  
4 Chappellaz, J., Clausen, H. B., Dahl-Jensen, D., Fischer, H., Fluckiger, J.,  
5 Fritzsche, D., Fujii, Y., Goto-Azuma, K., Gronvold, K., Gundestrup, N. S.,  
6 Hansson, M., Huber, C., Hvidberg, C. S., Johnsen, S. J., Jonsell, U., Jouzel, J.,  
7 Kipfstuhl, S., Landais, A., Leuenberger, M., Lorrain, R., Masson-Delmotte, V.,  
8 Miller, H., Motoyama, H., Narita, H., Popp, T., Rasmussen, S. O., Raynaud, D.,  
9 Rothlisberger, R., Ruth, U., Samyn, D., Schwander, J., Shoji, H., Siggard-  
10 Andersen, M. L., Steffensen, J. P., Stocker, T., Sveinbjornsdottir, A. E., Svensson,  
11 A., Takata, M., Tison, J. L., Thorsteinsson, T., Watanabe, O., Wilhelms, F.,  
12 White, J. W. C., and Project, N. G. I. C.: High-resolution record of Northern  
13 Hemisphere climate extending into the last interglacial period, *Nature*, 431, 147-  
14 151, 2004.
- 15 Bergamaschi, P., Hein, R., Heimann, M., and Crutzen, P. J.: Inverse modeling of the  
16 global CO cycle 1. Inversion of CO mixing ratios, *J. Geophys. Res. - Atmos.*, 105,  
17 1909-1927, 2000.
- 18 Buizert, C., Martinerie, P., Petrenko, V. V., Severinghaus, J., Trudinger, C., Witrant, E.,  
19 Rosen, J. L., Orsi, A. J., Rubino, M., Etheridge, D. M., Steele, L. P., Hogan, C.,  
20 Laube, J. C., Sturges, W. T., Levchenko, V., Smith, A. M., Levin, I., Conway, T.  
21 J., Dlugokencky, E. J., Lang, P. M., Kawamura, K., Jenk, T. M., White, J. W. C.,  
22 Sowers, T., Schwander, J., and Blunier, T.: Gas transport in firn: multiple-tracer  
23 characterisation and model intercomparison for NEEM, Northern Greenland,  
24 *Atmos. Chem. Phys.*, 12, 4259-4277, 2012.
- 25 Clark, I. D., Henderson, L., Chappellaz, J., Fisher, D., Koerner, R., Worthy, D. E. J.,  
26 Kotzer, T., Norman, A. L., and Barnola, J. M.: CO<sub>2</sub> isotopes as tracers of firn air  
27 diffusion and age in an Arctic ice cap with summer melting, Devon Island,  
28 Canada, *J. Geophys. Res. - Atmos.*, 112, D01301, doi:10.1029/2006JD007471,  
29 2007.
- 30 Colbeck, S. C.: Air Movement in Snow Due to Wind Pumping. *J. Glaciol.*, 35, 209-213,  
31 1989.
- 32 Colussi, A. J., and Hoffmann, M. R.: In situ photolysis of deep ice core contaminants by  
33 Cerenkov radiation of cosmic origin, *Geophys. Res. Lett.*, 30 (4), 1195,  
34 doi:10.1029/2002GL016112, 2003.
- 35 Duncan, B. N., Logan, J. A., Bey, I., Megretskaia, I. A., Yantosca, R. M., Novelli, P. C.,  
36 Jones, N. B., and Rinsland, C. P.: Global budget of CO, 1988-1997: Source  
37 estimates and validation with a global model, *J. Geophys. Res. - Atmos.*, 112,  
38 D22301, doi:10.1029/2007JD008459, 2007.
- 39 Grootes, P. M., Stuiver, M., White, J. W. C., Johnsen, S., and Jouzel, J.: Comparison of  
40 Oxygen-Isotope Records from the GISP2 and GRIP Greenland Ice Cores, *Nature*  
41 366, 552-554, 1993.
- 42 Haan, D., Martinerie, P., and Raynaud, D.: Ice core data of atmospheric carbon monoxide  
43 over Antarctica and Greenland during the last 200 years, *Geophys. Res. Lett.*, 23,  
44 2235-2238, 1996.

- 1 Haan, D., and Raynaud, D.: Ice core record of CO variations during the last two  
2 millennia: atmospheric implications and chemical interactions within the  
3 Greenland ice, *Tellus B*, 50, 253-262, 1998.
- 4 Novelli, P. C., Elkins, J. W., and Steele, L. P.: The Development and Evaluation of a  
5 Gravimetric Reference Scale for Measurements of Atmospheric Carbon  
6 Monoxide, *J. Geophys. Res. - Atmos.*, 96, 13109-13121, 1991.
- 7 Novelli, P. C., Masarie, K. A., and Lang, P. M.: Distributions and recent changes of  
8 carbon monoxide in the lower troposphere, *J. Geophys. Res. - Atmos.*, 103,  
9 19015-19033, 1998.
- 10 Novelli, P. C., Masarie, K. A., Lang, P. M., Hall, B. D., Myers, R. C., and Elkins, J. W.:  
11 Reanalysis of tropospheric CO trends: Effects of the 1997-1998 wildfires, *J.*  
12 *Geophys. Res. - Atmos.*, 108, (D15), 4464, doi:10.1029/2002JD003031, 2003.
- 13 Price, H., Jaegle, L., Rice, A., Quay, P., Novelli, P. C., and Gammon, R.: Global budget  
14 of molecular hydrogen and its deuterium content: Constraints from ground  
15 station, cruise, and aircraft observations, *J. Geophys. Res. - Atmos.*, 112,  
16 D22108, doi:10.1029/2006JD008152, 2007.
- 17 Rommelaere, V., Arnaud, L., and Barnola, J. M.: Reconstructing recent atmospheric trace  
18 gas concentrations from polar firn and bubbly ice data by inverse methods. *J.*  
19 *Geophys. Res. - Atmos.*, 102, 30069-30083, 1997.
- 20 Schwander, J.: The transformation of snow to ice and the occlusion of gases, in: *The*  
21 *Environmental Record in Glaciers and Ice Sheets* (H. Oeschger, and C. Langway,  
22 Eds.), pp. 53-67. John Wiley, New York, 1989.
- 23 Severinghaus, J. P., and Battle, M. O.: Fractionation of gases in polar ice during bubble  
24 close-off: New constraints from firn air Ne, Kr and Xe observations, *Earth Planet.*  
25 *Sci. Lett.*, 244, 474-500, 2006.
- 26 Severinghaus, J. P., Grachev, A., and Battle, M.: Thermal fractionation of air in polar firn  
27 by seasonal temperature gradients, *Geochem. Geophys. Geosy.*, 2,  
28 2000GC000146, 2001.
- 29 Sowers, T., Bender, M., Raynaud, D., and Korotkevich, Y. S.: Delta-N-15 of N<sub>2</sub> in Air  
30 Trapped in Polar Ice - a Tracer of Gas Transport in the Firn and a Possible  
31 Constraint on Ice Age - Gas Age Differences, *J. Geophys. Res. - Atmos.*, 97,  
32 15683-15697, 1992.
- 33 Vinther, B. M., Clausen, H. B., Johnsen, S. J., Rasmussen, S. O., Andersen, K. K.,  
34 Buchardt, S. L., Dahl-Jensen, D., Seierstad, I. K., Siggaard-Andersen, M. L.,  
35 Steffensen, J. P., Svensson, A., Olsen, J., and Heinemeier, J.: A synchronized  
36 dating of three Greenland ice cores throughout the Holocene, *J. Geophys. Res. -*  
37 *Atmos.*, 111, D13102, doi: 10.1029/2005jd006921, 2006.
- 38 Vollmer, M. K., Walter, S., Bond, S. W., Soltic, P., and Rockmann, T.: Molecular  
39 hydrogen (H<sub>2</sub>) emissions and their isotopic signatures (H/D) from a motor  
40 vehicle: implications on atmospheric H<sub>2</sub>, *Atmos. Chem. Phys.*, 10, 5707-5718,  
41 2010.
- 42 Witrant, E., Martinerie, P., Hogan, C., Laube, J. C., Kawamura, K., Capron, E., Montzka,  
43 S. A., Dlugokencky, E. J., Etheridge, D., Blunier, T., and Sturges, W. T.: A new  
44 multi-gas constrained model of trace gas non-homogeneous transport in firn:  
45 evaluation and behavior at eleven polar sites, *Atmos. Chem. Phys. Disc.*, 11,  
46 23029 - 23080, 2011.
- 47



1

<b>Borehole</b>	<b>Sampling Period</b>	<b>Gas</b>	<b>Laboratory</b>
NEEM EU	July 2008	CO	NOAA, CSIRO, Heidelberg, Stony Brook*
		H <sub>2</sub>	NOAA, CSIRO
NEEM US	July 2008	CO	NOAA, Heidelberg
		H <sub>2</sub>	NOAA, Heidelberg*
NEEM S4	July 2008	CO	UEA*
		H <sub>2</sub>	UEA*
Summit	May - June 2006	CO	NOAA
NGRIP	May - June 2001	CO	NOAA

2

3

4

5

6

7

8

9

Table S1. A summary of the Greenland firn air CO and H<sub>2</sub> measurements presented in this paper. Data sets that were not included in the final atmospheric history reconstructions are marked by \* next to the name of the measurement laboratory.

1

	<b>[CO], nmol mol<sup>-1</sup></b>	<b>[H<sub>2</sub>], nmol mol<sup>-1</sup></b>
Direct flask fill	4.0	800.1
Direct flask fill	4.5	798.4
Through US system	3.8	804.7
Through US system	3.8	803.5
Through EU system	4.5	809.2
Through EU system	5.1	801.5

2

3

Table S2. Results of the procedural blank tests conducted during NEEM firn air sampling; measurements were performed at NOAA.

4

5

6

1

NEEM EU 2008		NEEM US 2008		Summit 2006		NGRIP 2001	
Depth, m	[CO]	Depth, m	[CO]	Depth, m	[CO]	Depth, m	[CO]
0.00	88.3	0.00	93.9	0.00	129.4	0.30	117.2
4.90	106.3	2.85	94.2	15.05	143.9	2.40	128.7
10.10	134.3	5.23	128.5	25.00	139.2	4.97	132.3
14.80	133.7	9.83	129.8	29.96	133.8	7.50	136.2
19.75	135.9	19.30	134.8	39.92	133.8	10.05	141.1
27.54	136.8	34.70	132.8	50.00	134.8	14.95	142.4
34.72	134.8	49.70	130.5	58.00	136.3	20.00	138.9
50.00	132.8	57.47	137.2	63.00	136.1	27.43	135.8
57.40	134.3	59.90	137.3	65.89	137.3	34.63	134.6
59.90	135.9	62.00	136.3	67.95	136.8	42.57	136.5
61.95	135.2	64.03	142.2	70.13	138.0	55.14	141.0
63.85	140.4	65.50	144.5	72.17	144.9	59.35	141.3
65.75	146.1	66.90	151.0	74.30	150.1	62.30	142.2
68.05	154.5	68.30	154.8	76.00	153.2	65.02	142.7
70.05	157.0	69.80	155.8	78.00	151.2	66.99	145.0
72.00	152.4	71.40	152.0	79.94	148.8	69.04	150.3
74.08	146.7	72.85	145.9			71.75	153.0
75.90	141.7	73.80	143.6			74.30	148.2
77.75	135.9	75.60	138.5			76.70	143.7
						77.68	138.6

2

3

4 Table S3. Finalized, depth-averaged firn air [CO] data (in nmol mol<sup>-1</sup>) from all boreholes  
5 that were used for atmospheric [CO] reconstructions. All data are on the WMO 2004  
6 [CO] scale.

1

	<b>Alert - Summit</b>	<b>Alert - Barrow</b>	<b>Alert - Ny Alesund</b>
<b>Period of overlap</b>	Jul 1997 - Dec 2008 (large gaps)	Apr 1992 - Dec 2008	Feb 1994 - Dec 2008
<b>Mean offset</b>	0.2	-1.3	-1.8
<b>January</b>	12.7	-0.3	0.0
<b>February</b>	4.7	-2.8	1.1
<b>March</b>	5.8	-0.7	0.3
<b>April</b>	9.2	0.3	0.7
<b>May</b>	7.8	-0.1	1.8
<b>June</b>	-2.1	-2.2	-0.9
<b>July</b>	-8.7	-2.7	-1.4
<b>August</b>	-13.7	-3.5	-4.7
<b>September</b>	-6.0	-4.0	-3.5
<b>October</b>	-1.0	-1.3	-3.0
<b>November</b>	-1.7	0.6	-5.6
<b>December</b>	3.4	2.0	-6.6

2

3

4

5

6

7

Table S4. Comparison of [CO] offsets between NOAA Arctic flask sampling stations. The overall mean offset and the average offset for each month are calculated based on monthly data downloaded from <ftp://ftp.cmdl.noaa.gov/ccg>.

1

	CO	H <sub>2</sub>
TOTAL SOURCE, Tg /yr	2236-2489	73
Source or sink partitioning, % of total		
SOURCES		
Fossil fuels	~20%	~25%
Biofuels	~8%	~6%
Biomass burning	~22%	~14%
N <sub>2</sub> fixation in ocean	0%	~8%
Methane oxidation	~35%	~34%
Biogenic NMHC oxidation	~16%	~13%
SINKS		
OH	~90%	~25%
Soils	~10%	~75%

2

3

4

5

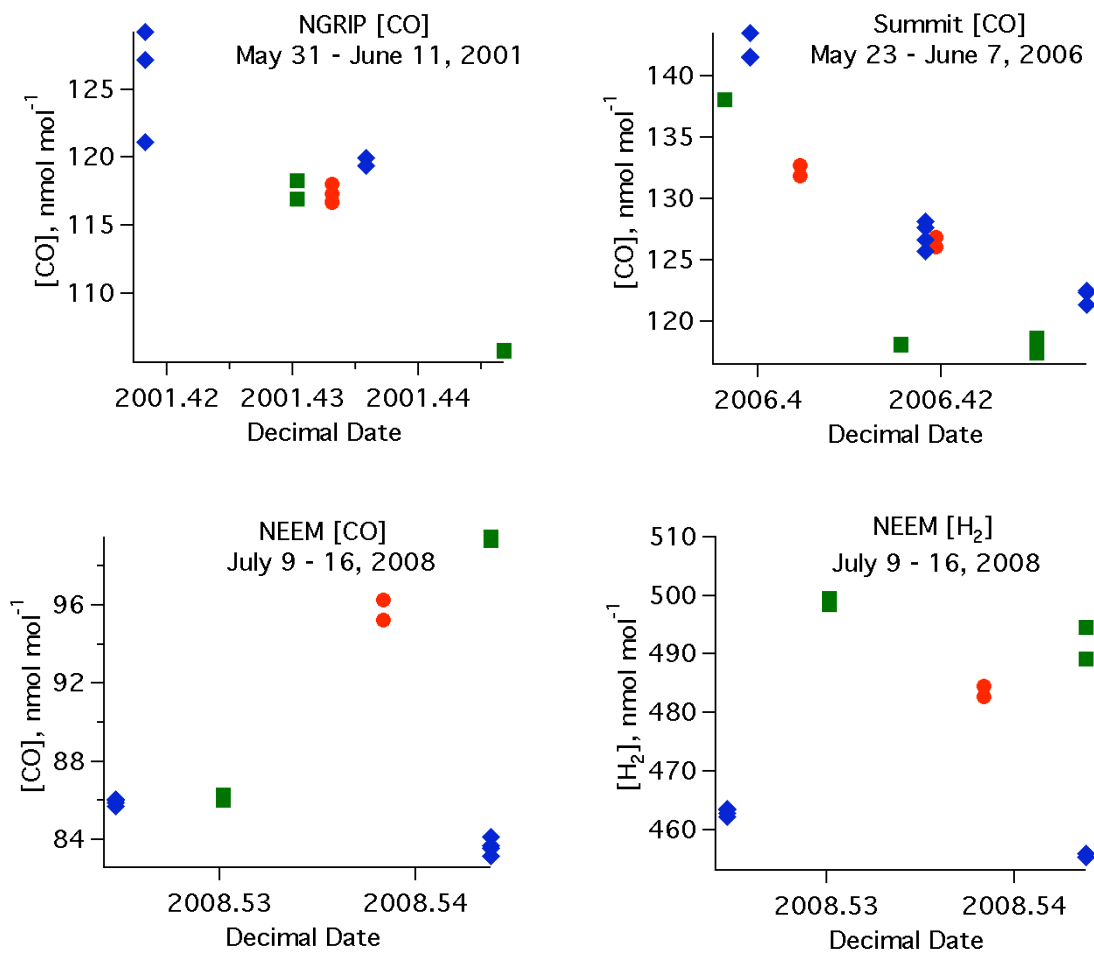
6

7

8

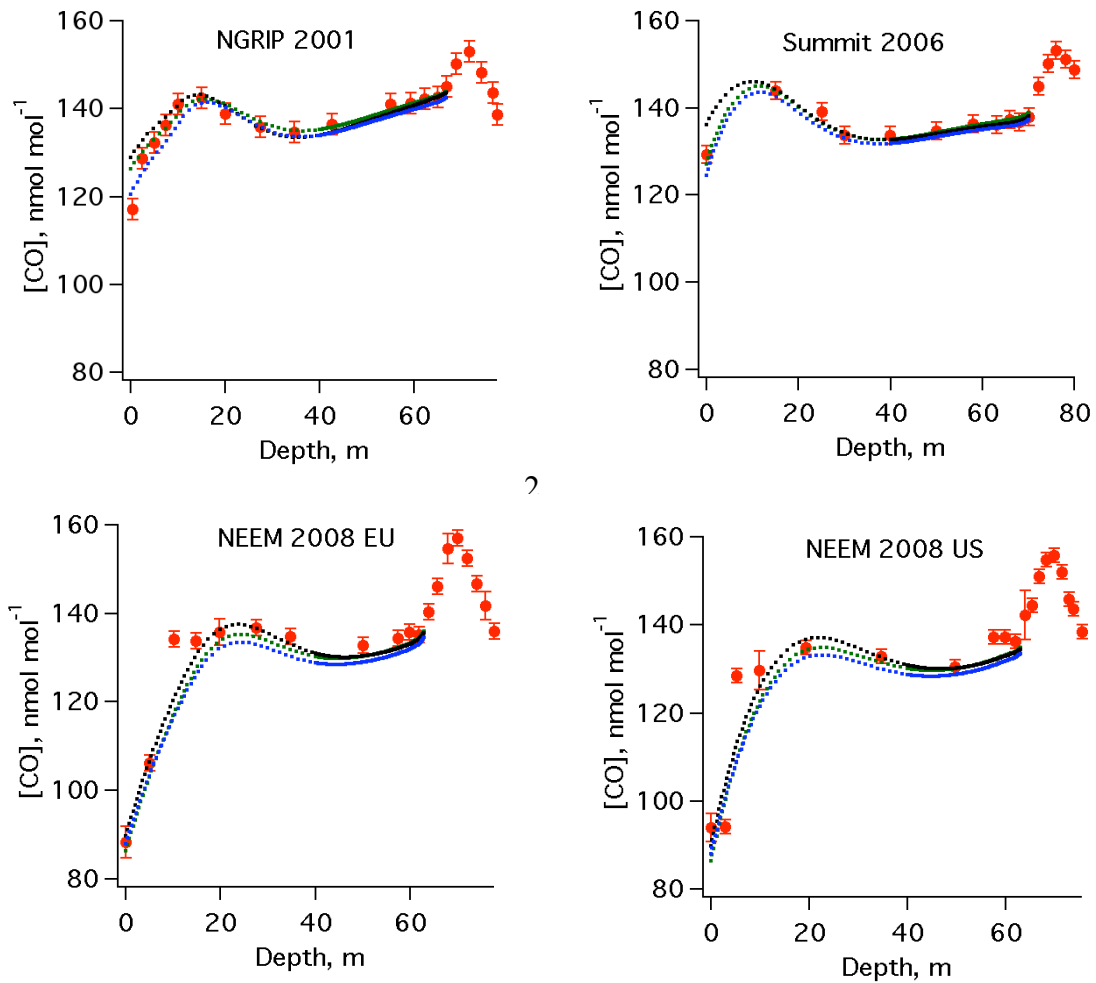
9

Table S5. Estimates of global sources and sinks of CO and H<sub>2</sub>. CO budget is as in Duncan et al. (2007). OH and soil sinks for CO are from Bergamaschi et al. (2000) as listed in Table 2 of Duncan et al. (2007). H<sub>2</sub> budget is as in Price et al. (2007). The fossil fuel, biofuel and biomass burning terms also include CO and H<sub>2</sub> produced from oxidation of VOCs released from these combustion sources.



1  
2  
3  
4  
5  
6  
7  
8  
9  
10

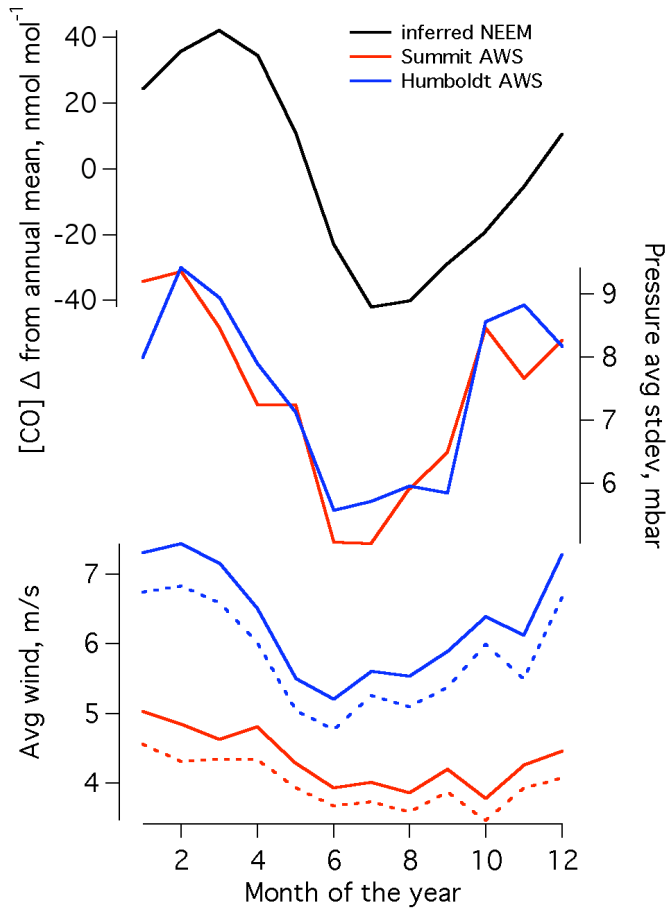
Figure S1. [CO] and [H<sub>2</sub>] comparisons of surface flasks filled through the firn air systems with NOAA flask measurements from the two closest monitoring stations during the same time period. Red circles: surface air samples from firn sampling sites; green squares: NOAA Summit data; blue diamonds: NOAA Alert data. All [CO] data are on WMO 2004 scale, all [H<sub>2</sub>] data are on NOAA scale. Note that large short-term fluctuations are not uncommon for these gases (especially for CO).



2

3  
4  
5  
6  
7  
8  
9  
10  
11  
12  
13  
14  
15  
16  
17  
18  
19  
20  
21

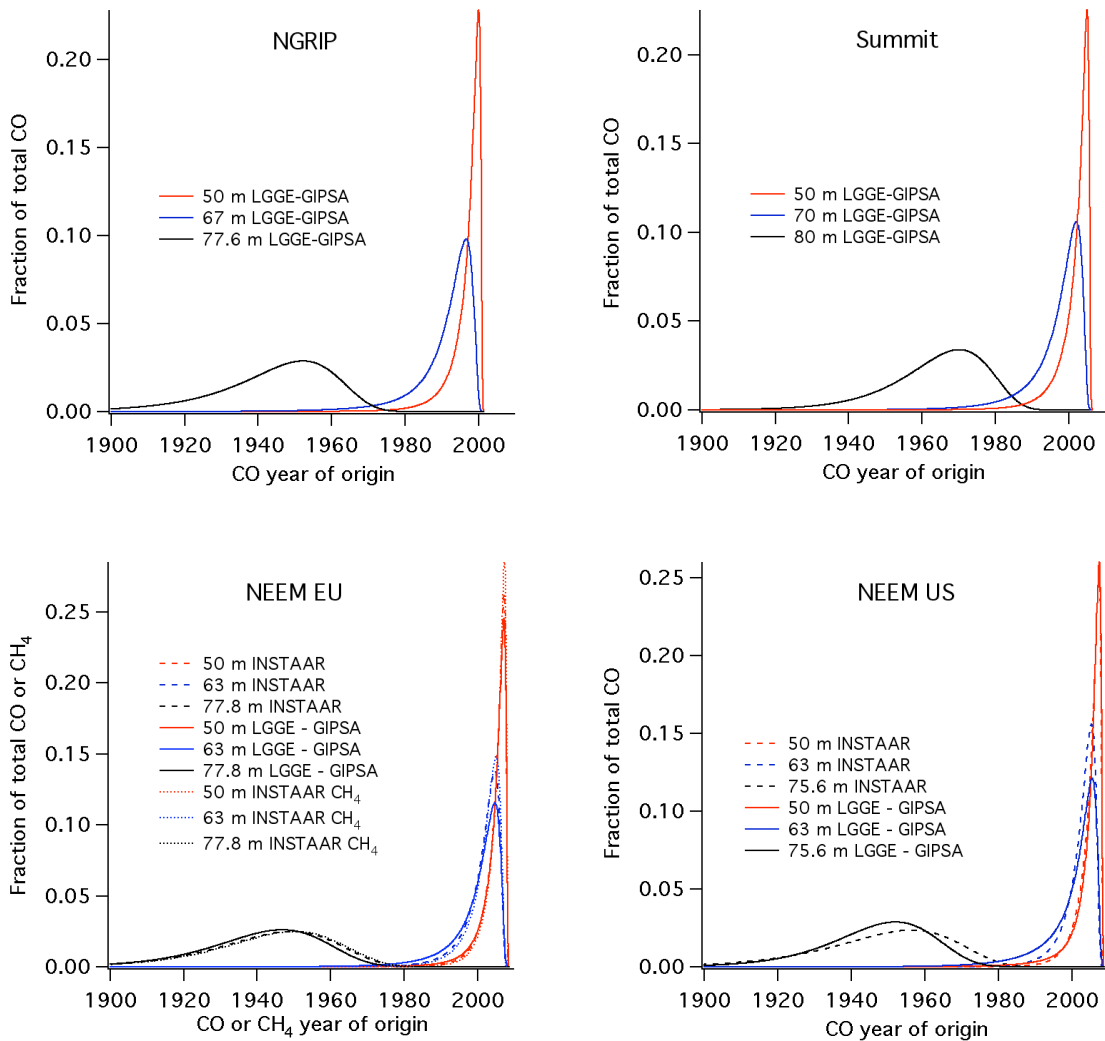
Figure S2. Comparison of firm [CO] data with firm forward model runs (LGGE-GIPSA model) using NOAA atmospheric histories. Data are in red (WMO-2004 scale, with uncertainties). Color scheme for model runs: Barrow history – black; Alert history – blue; Ny Alesund history – green. As discussed in the text, the comparison is most valid in the depth range between 40 m (below seasonal cycle influences) and the start of the lock-in zone; model output is shown with solid lines in this depth range and with dotted lines above this depth range.



1  
2  
3  
4  
5  
6  
7  
8  
9  
10  
11  
12  
13  
14

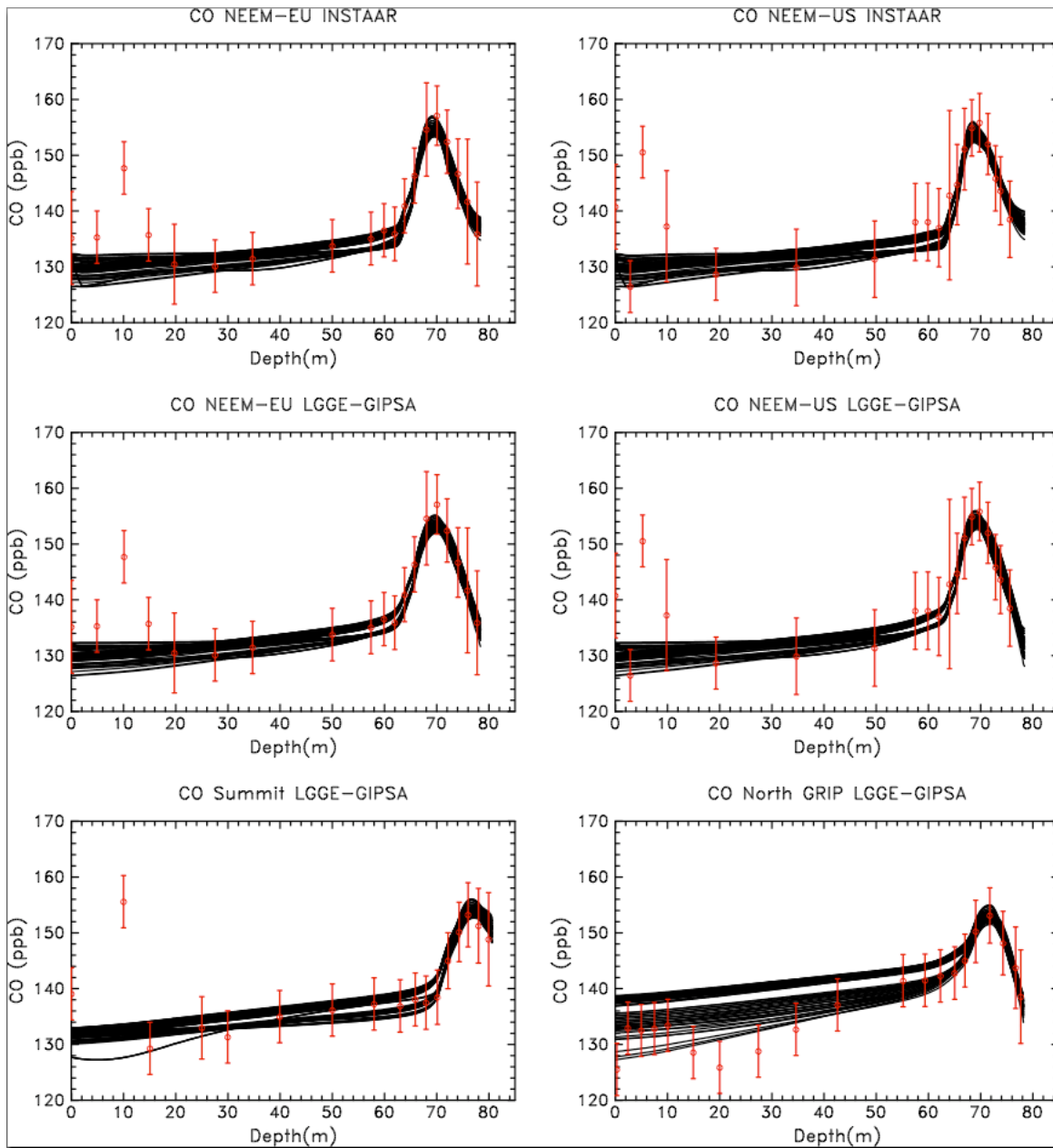
Figure S3. The seasonal variability of [CO], surface pressure and wind at Greenland sites. The monthly [CO] deviation from mean annual is estimated for NEEA, based on the existing NOAA Alert and Summit records up through 2008 (<ftp://ftp.cmdl.noaa.gov/ccg>). “Pressure avg stdev” is a measure of surface pressure variability and is calculated by finding the standard deviation of pressure values for each month, then averaging these standard deviation values over all Januarys, Februarys, etc. Each AWS has two wind speed gauges, and average wind speed from the 2<sup>nd</sup> gauge is plotted as a dotted line. Both Summit and Humboldt AWS records start in 1996. Humboldt wind data before 1996.35 and pressure data from May 1999 were excluded because of problems with gauges.





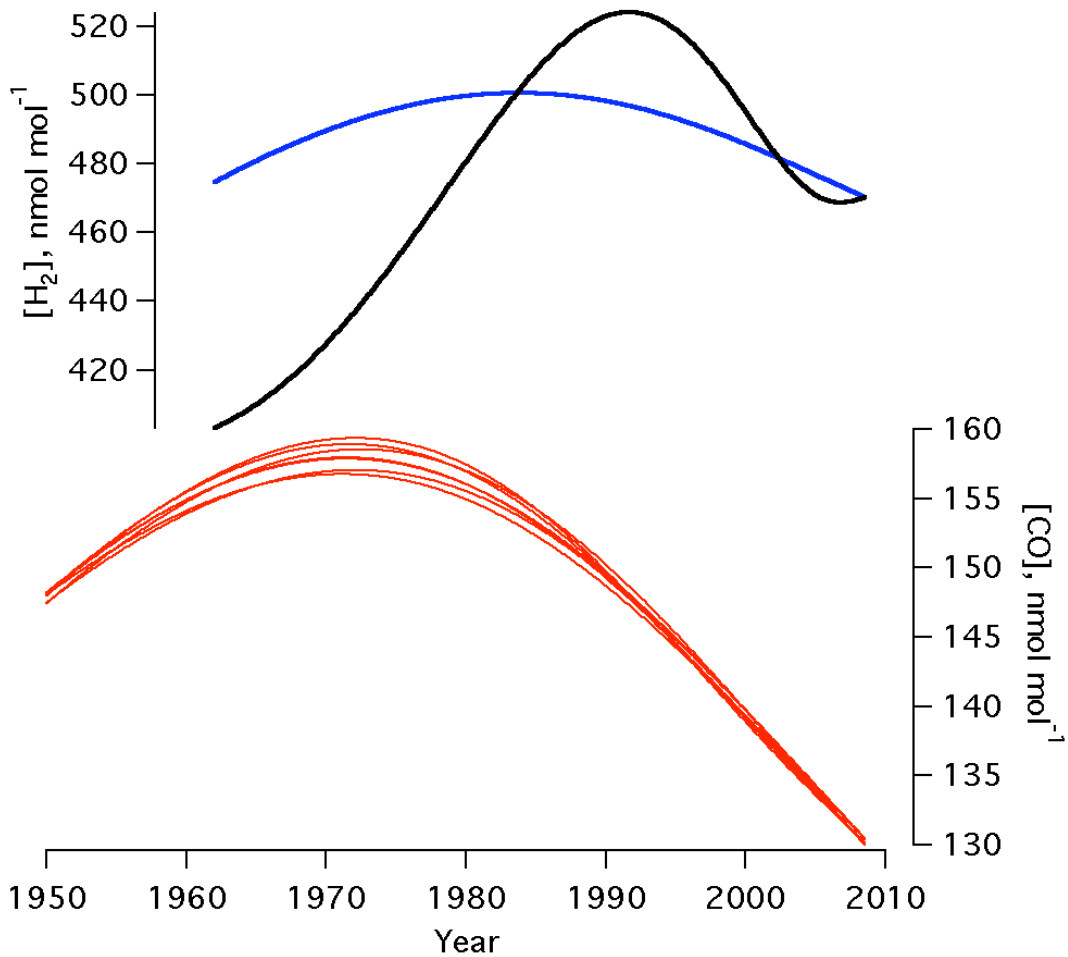
1  
2  
3  
4  
5  
6  
7  
8  
9  
10

Figure S4. CO age distributions predicted by the LGGE-GIPSA and INSTAAR forward models for the different boreholes. For each borehole, curves are shown for one depth above the lock-in zone (red), one depth right near the start of the lock-in zone (blue), as well as the deepest sampled depth (black). The CH<sub>4</sub> age distributions predicted by the INSTAAR model are also shown for the example of NEEM EU borehole. As can be seen, the INSTAAR model CO age distributions are almost indistinguishable from the INSTAAR model CH<sub>4</sub> age distributions, demonstrating the validity of the CO-CH<sub>4</sub> comparison in Figure 6.



1  
2  
3  
4  
5  
6

Figure S5. Convolutions of the 61 successful [CO] scenarios with the transfer functions for individual forward models and boreholes. The error bars are the full uncertainties for the data-model comparisons as described in Section 4.2 of main text. Upper firm [CO] data are corrected for seasonality.



1  
 2 Figure S6. [H<sub>2</sub>] reconstructions from NEEM firn plotted together with [CO]  
 3 reconstructions. Because the [H<sub>2</sub>] reconstructions are only done to indicate an oldest-  
 4 possible peak date for [H<sub>2</sub>] over Greenland, fewer inversions were performed, and only  
 5 with data from the NEEM EU borehole. The black line is an inversion based on the  
 6 LGGE-GISPA model transfer function that provides the best fit to the data; the blue line  
 7 is a corresponding inversion using the INSTAAR model transfer function. As can be  
 8 seen, [H<sub>2</sub>] reconstructions are much more model-dependent than for [CO]. For  
 9 comparison, the subset of successful [CO] scenarios reconstructed also using only NEEM  
 10 EU borehole data only are shown in red.